

Experimental entanglement generation for quantum key distribution beyond 1 Gbit/s

Sebastian Philipp Neumann,^{*} Mirela Selimovic, Martin Bohmann, and Rupert Ursin[†]
Institute for Quantum Optics and Quantum Information Vienna, Boltzmanngasse 3, 1090 Vienna
Vienna Center for Quantum Science and Technology, Boltzmanngasse 5, 1090 Vienna, Austria
 (Dated: July 7, 2022)

Top-performance sources of photonic entanglement are an indispensable resource for many applications in quantum communication, most notably quantum key distribution. However, up to now, no source has been shown to simultaneously exhibit the high pair-creation rate, broad bandwidth, excellent state fidelity, and low intrinsic loss necessary for gigabit secure key rates. In this work, we present for the first time a source of polarization-entangled photon pairs at telecommunication wavelengths that covers all these needs of real-world quantum-cryptographic applications, thus enabling unprecedented quantum-secure key rates of more than 1 Gbit/s. Our source is designed to optimally exploit state-of-the-art telecommunication equipment and detection systems. Any technological improvement of the latter would result in an even higher rate without modification of the source. We discuss the used wavelength-multiplexing approach, including its potential for multi-user quantum networks and its fundamental limitations. Our source paves the way for high-speed quantum encryption approaching present-day internet bandwidth.

I. INTRODUCTION

Entanglement-based quantum key distribution (QKD) requires sources of photonic entanglement that exhibit high overall pair creation rates, high spectral brightness, low intrinsic loss, high fidelity to maximally entangled states and low maintenance. These points are getting ever more important for achieving non-vanishing key rates over fiber and free-space quantum links which are governed by unavoidable strong losses. In order to achieve this, different source designs have achieved remarkable individual figures of merit: Atzeni et al. [1] achieved 2.2×10^9 cps/mW overall brightness and Sun et al. [2] 1.2×10^9 cps/mW/nm spectral brightness, both in waveguide configurations. Liu et al. [3] reported an average collection efficiency of 84.1%, Kaiser et al. [4] as well as Joshi [5] showed 99.8% polarization visibility and the source of Tang et al. [6] even survived a rocket explosion. For a recent comprehensive overview and a detailed discussion of the parameters in use, see Ref.s [7, 8].

While all of the reported sources show excellent merits regarding one or even two of these fundamental parameters, none of them exhibit outstanding overall performance necessary for first-grade real-world QKD applications. In such applications, high *overall brightness* is necessary to create high key rates required in telecommunication infrastructures today. It is defined as the number of entangled photon pairs created in the source before all losses. High *spectral brightness*, i.e. the rate of photon pairs created per wavelength, enables efficient wavelength division multiplexing (WDM) of signals [9, 10], diminishes dispersion effects [11] and will be necessary to couple to quantum memories in the future [12]. *Collection efficiency* is the probability of a photon created

in the source being detected. High source-intrinsic collection efficiency allows to tolerate more (unavoidable) channel loss. High *visibility* of the entangled state allows the experimenter to efficiently perform error correction and privacy amplification in post-processing, which means that a larger fraction of the raw key can be utilized; additionally it can partly compensate for noise, detector jitter and channel loss.

The highest experimentally generated key rates as of today were acquired under laboratory conditions, without deployment of real-life links. The record values are 10 Mbit/s [13] in a decoy-state configuration, 26.2 Mbit/s [14] using time-bin qudits and 7.0 Mbit/s [15] in an implementation with high-dimensional entanglement.

In this work, we present a source of polarization-entangled photon pairs performing competitively in all of the above-mentioned parameters, enabling unprecedented key rates beyond 1 Gbit/s by exploiting polarization entanglement only. The source was built in a bulk Sagnac-loop configuration deploying type-0 spontaneous parametric down-conversion (SPDC) inside a nonlinear crystal producing polarization-entangled photon pairs at telecom wavelength. Using bulk polarization measurement modules and a tunable blazed-grating filter, respectively, we quantified brightness, collection efficiency, spectral bandwidth and polarization visibility for different WDM channels as well as the full spectrum. We find that using 66 channel pairs of off-the-shelf WDM devices, the source could supply a total of 1.1 Gbit/s secure key in a point-to-point configuration. Even higher values of up to 3.6 Gbit/s are conceivable when using narrow ultra-dense WDM channels and pumping with high laser power. Additionally, we show that by using the full 106 nm-bandwidth spectrum of our source, a fully connected local quantum network with up to 33 users could be created. Our results provide an essential contribution towards high-key-rate quantum communication necessary for future quantum infrastructures.

^{*} sebastian.neumann@oeaw.ac.at

[†] rupert.ursin@oeaw.ac.at

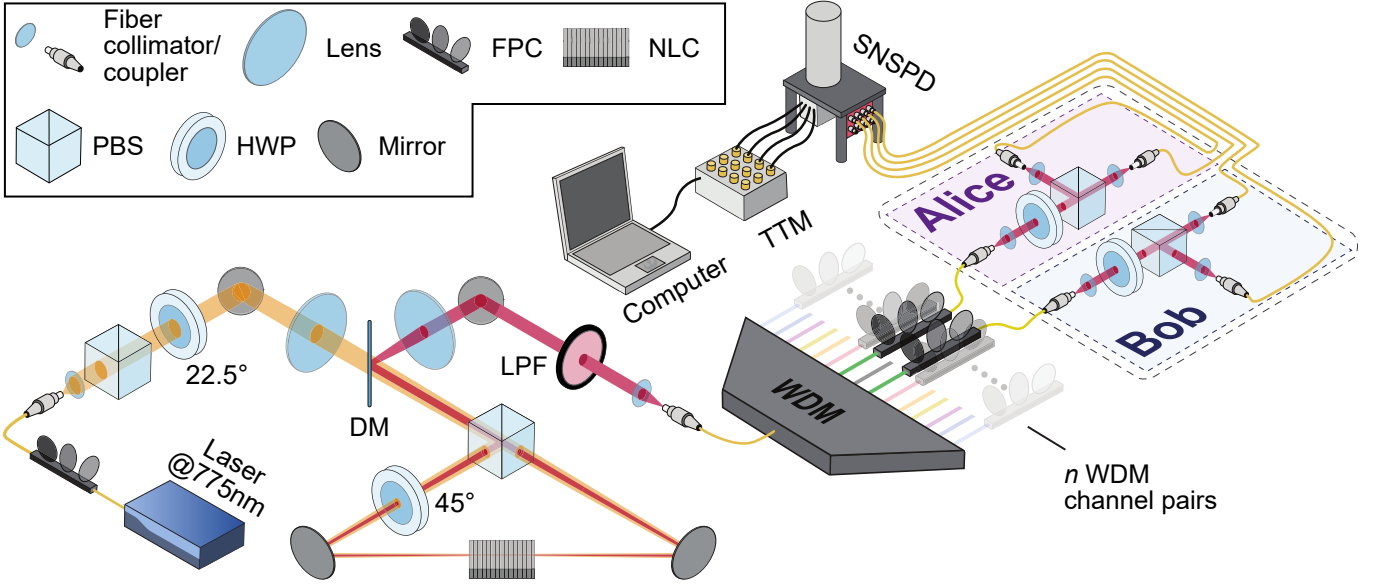


FIG. 1. Sketch of the setup. The continuous-wave pump laser at 775.06 nm is coupled into a single-mode fiber (SMF) and directed towards the bulk optics setup. After beam collimation, a polarizing beam splitter (PBS) and a half-wave plate (HWP) set the pump laser's polarization to 45° . A pump lens bidirectionally focuses the pump into the nonlinear crystal (NLC) placed inside a Sagnac loop. The loop consists of a dichroic PBS splitting the pump by transmitting (reflecting) the horizontally (vertically) polarized part. The reflected part passes a HWP at 45° . Thus, all pump photons are horizontally polarized when entering the NLC, where photon pairs are created via type-0 spontaneous parametric down-conversion (SPDC). They travel back to the PBS, where both propagation direction modes interfere and the SPDC photons' polarization states become entangled. Successively, a dichroic mirror (DM) separates the SPDC beam from the pump. The SPDC traverses a longpass filter (LPF) blocking residual pump light before being collected by a SMF. The broad total photon spectrum is subdivided by use of a WDM. For visibility measurements, polarization rotations in the fiber have to be compensated using fiber polarization controllers (FPC) in order to acquire the desired correlations. Measurements in mutually unbiased bases are realized by setting both receiver's HWP to either 0° or 22.5° . The PBS output modes are coupled into SMF and directed to four channels of superconducting nanowire single-photon detectors (SNSPD), whose detection times are registered using a time-tagging module (TTM) and post-processed with a computer. For measurements of brightness and collection efficiency, the WDMs are directly connected to the SNSPDs. For the measurement of the total spectrum, the WDM was replaced by a 50:50 beam splitter, one arm of which was connected to a tunable filter (not depicted) before detection.

II. RESULTS

To arrive at > 1 Gbit/s key rates, we need to determine the outstanding values of the source's spectral bandwidth, collection efficiency, brightness and visibility values, which we will set forth in the following. The experimental set-up is depicted in Fig. 1. The source was built in a bulk Sagnac configuration with the loop containing a type-0 nonlinear crystal (NLC). It was bidirectionally pumped using a 775.06 nm continuous-wave laser with its focusing parameters optimized for high-brightness SPDC. It produces telecom-wavelength entangled photon pairs with their spectrum centered around 1550.12 nm. Carefully chosen collimation and coupling optics allow for the SPDC's low-loss insertion into a single-mode fiber. For a more detailed description of the source's working principle, see the caption of Fig. 1 and the Methods section. The photons were detected by use of two fiber-coupled superconducting nanowire single-photon detector (SNSPD) channels connected to a time-tagging module (TTM). From its time stamps, our com-

puter software calculated $g^{(2)}$ correlations between the channels, from which we identify the entangled photon pairs.

Figure 2 shows the source's collection efficiency over the full SPDC spectrum. The graph was acquired by probabilistically separating the entangled pairs with a 50:50 in-fiber beam splitter before detection and using a grating-based tunable wavelength filter in one of its arms. The spectrally resolved collection efficiency is required to quantify the portion of the spectrum usable in QKD. The source spectrum can be optimally exploited for QKD by deterministically separating entangled photon pairs using WDM channels. Due to energy conservation during the SPDC process, entangled photons are found in channel pairs equidistant from the spectrum's central wavelength. Such pairs are depicted in the same colors in Fig. 2. Each of the n channel pairs can be considered an independent carrier of photonic entanglement [16].

To precisely determine collection efficiencies and brightness values, matching WDM channel pairs were connected directly to the SNSPDs. To ensure straightforward comparability with other source designs, we did

not subject the photon pairs to long-distance link attenuation. The single-mode fibers in use added up to no more than 10 m length. All of the following collection efficiencies include coupling and transmission losses of WDMs and fibers as well as SNSPD detection efficiencies. We define the collection efficiency η , sometimes called “heralding” or “Klyshko” [17] efficiency, as $\eta = CC/\sqrt{S_A \cdot S_B}$, where CC are the coincident counts between the communicating partners’ detectors with single count rates S_A and S_B . Figure 3 shows collection efficiency values for different standard WDM channels of 100 and 200 GHz (dense WDM) and 2500 GHz (coarse WDM). Collection efficiencies stay above 20% on average in a 56.3 nm range around the central SPDC wavelength. As a comparison, averaging over the full spectral range, the value decreases to 12.9%. This value was acquired using a 50:50 in-fiber beam splitter and is in accordance with Fig. 2, since coupling into the collecting single-mode fiber is less efficient far from the central wavelength due to chromatic aberration of the coupling optics and wavelength-depended mode structures.

Figure 4 shows spectral brightness values, i.e., the number of photon pairs per pump power, wavelength and time, for the same WDM channels as used for Fig. 3. Solid lines refer to *detected* pair rates, while faint lines are calculated pair creation rates in the crystal before any loss. This parameter is called spectral brightness B . The latter depends on measured pair rates and collection efficiencies as $B = CC/\eta^2$. The highest spectral brightness value of $B_{31+37} = 4.17 \times 10^6$ cps/mW/nm was found in the 200 GHz WDM channel pair 31+37.

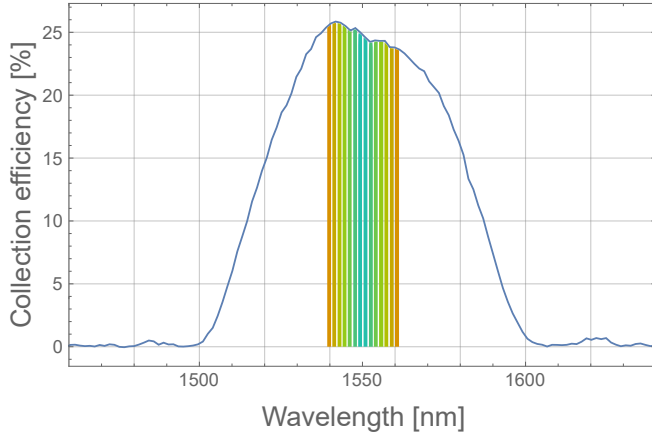


FIG. 2. Measured collection efficiency of the source per wavelength. The measurement was carried out using a tunable wavelength filter based on a rotatable blaze grating, which one photon of a pair passed. The graph was obtained by determining the ratio of coincidence counts vs. singles of the lossy filter arm and normalizing to the highest collection efficiency obtained in the WDM measurements (see Fig. 3). WDM channel pairs carrying entangled photon pairs are shown as slices of the same color. The slight asymmetry of the spectrum can be explained by varying coupling efficiencies of the tunable filter and the single-photon detectors.

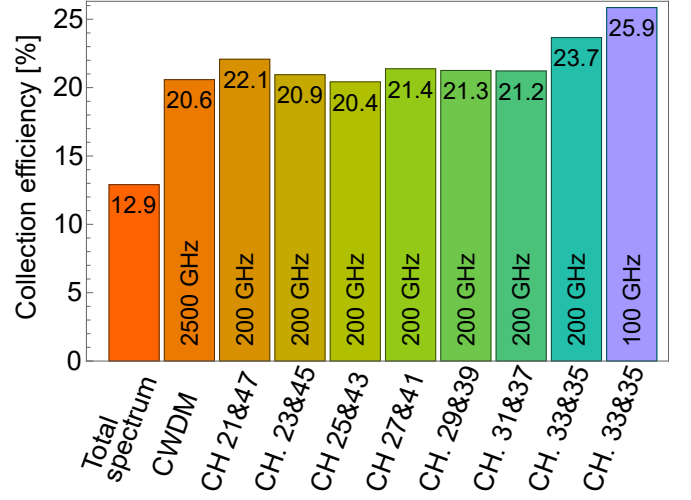


FIG. 3. Average measured collection efficiencies obtained by determining the ratio between coincident and single detector counts. Note that the lower values for the full spectrum originate in part from the fact that a probabilistic beam splitter was used to separate the photons, and in part from the fact that far from the central wavelength, the source intrinsically shows lower collection efficiencies due to its focusing parameters [18].

Figure 5 demonstrates our source’s exceptional fidelity to a maximally entangled state with measured polarization visibilities V of up to 99.4% in two mutually unbiased bases. To arrive at these values, bulk polarizing beam splitters with single-mode coupled output ports were implemented between WDMs and SNSPDs (cf. Fig. 1). V stayed above 99.2% for all observed 100 and 200 GHz channels. Since polarization rotations in fiber are wavelength dependent, no full polar-

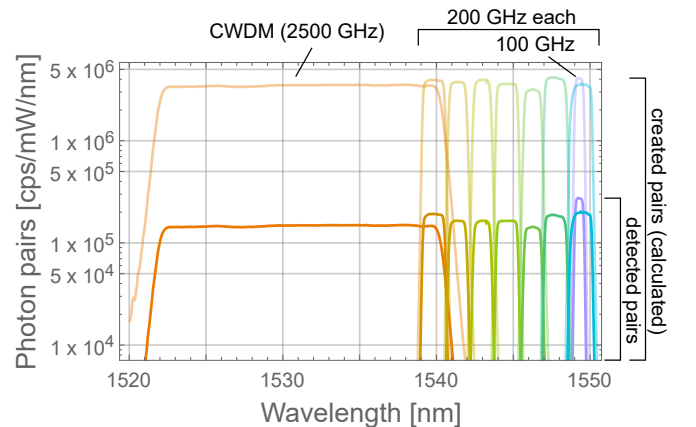


FIG. 4. Brightness values (transparent) and measured coincidences (solid) of the source for measured WDM channel pairs per mW. The central wavelength is 1550.12 nm, and only the channels with the lower wavelength of each channel pair are depicted for simplicity. Brightness values were calculated from measured coincidences and collection efficiencies.

ization compensation using fiber polarization controllers (FPC) can be achieved for broad spectra. However, even for the broader coarse WDM (CWDM) channels and the full spectrum, the quantum bit error rate (QBER) $E = (100\% - V)/2$ stays above the 11% limit necessary for secure key creation [19].

As a final figure of merit, we want to point out our source's stability: All of the above data was taken more than 6 months after source alignment, with no certifiable performance degradation during this period. The only active stabilization necessary was carried out by an electronically controlled oven restricting crystal temperature fluctuations to $< 0.01^\circ\text{C}$, while no performance degradation could be observed for changes $< 0.1^\circ\text{C}$.

From this experimental data, maximum secure key rates can be inferred according to the model in Ref. [8]. The source can be operated as is, by optimizing the laser power inside the crystal. This optimum is governed by the wavelength-channel width, leading to a trade-off between the rate of detected photon pairs and the accidental detection probability per wavelength-channel pair. Using the collection efficiency, brightness, and visibility values experimentally achieved in our experiment, we simulate QKD implementations with different WDM scenarios in Fig. 6. Here, each WDM-channel pair can provide a secure key rate R_k^s depending on its individual collection efficiency and entanglement quality. In this work, we are concerned with the total key rate $R^s = \sum_{k=1}^n R_k^s$ achievable with n channel pairs from our source. Our calculations, depicted in Fig. 6, show that already with standard off-the-

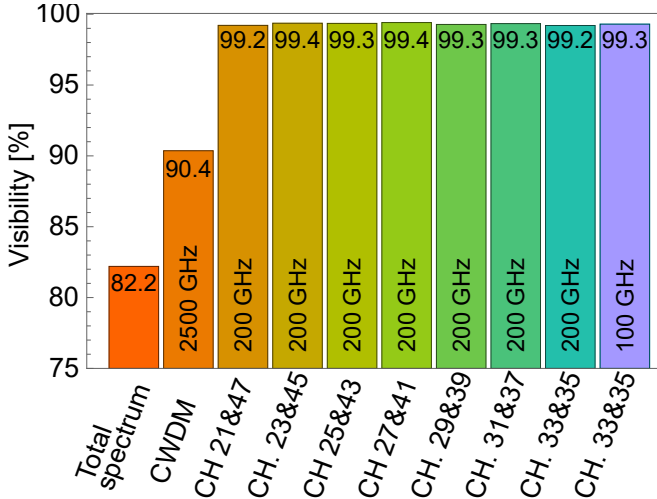


FIG. 5. Average values of visibility V obtained by measuring correlations in polarization in two mutually unbiased bases. We measured $V > 99.2\%$ for all WDM spectral widths used for key calculations. We attribute lower visibility values for the 2500 GHz coarse WDM (CWDM) and the full spectrum to wavelength-dependent polarization rotations in the fibers, which can be compensated individually if subdividing in narrow spectra.

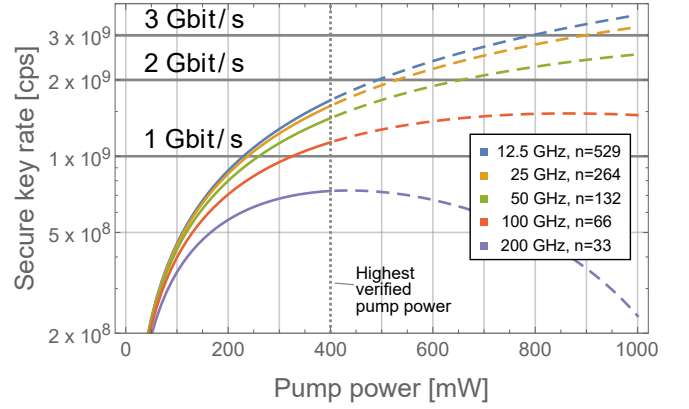


FIG. 6. Expected secure key rates per pump power of our source for different wavelength demultiplexing scenarios. The WDM channels under consideration follow standards defined by the International Telecommunication Union and we indicate the number of used channel pairs n . Already for 100 GHz channels, our source could provide key rates above 1 Gbit/s. While we experimentally verified laser-damage free source-operation up until 400 mW pump power, it is reasonable to assume that 1000 mW are still feasible [20]. This could allow for more than 2 Gbit/s in a 50 GHz demultiplexing scheme, while 25 GHz and 12.5 GHz enable more than 3 Gbit/s. The relative increase in key rate for ever narrower channels becomes smaller due to the accompanying increase of the entangled photons' coherence time.

shelf 100 GHz WDM channels, 1.15 Gbit/s secure key rate could be achieved at 400 mW pump power when deploying suitable high-end detectors. With 132 channels of 50 GHz width, $R^s = 2$ Gbit/s can be achieved with 660 mW pump power. 25 GHz channels would even allow for 3 Gbit/s at 900 mW, and reducing the spacing further to 529 channel pairs of 12.5 GHz, the same key rate value could be reached already with 800 mW pump power. When pumping with 1000 mW in the latter WDM configuration, a maximum value of 3.6 Gbit/s is possible.

III. DISCUSSION

We have presented a stable source of polarization-entangled photon pairs with high total and spectral brightness, high collection/heralding efficiency and extremely high state fidelity. Calculating the quantum secure key rates that our source could sustain when operating with sufficiently performing single-photon detectors, we arrive at key rates above 1 Gbit/s with off-the-shelf wavelength-division-multiplexing devices and laser powers below the crystal's damage threshold. When relaxing the latter requirements, key rates of more than 3 Gbit/s are conceivable with our state-of-the-art source:

Firstly, stronger pump laser power could increase the effective spectral and overall brightness. To mitigate the risk of damage to our setup, we restricted ourselves to powers of no more than 400 mW. However, if one were

to install laminar airflow boxes to keep dust away from the optical surfaces, specifications by the crystal manufacturer suggest that powers of 1 W and beyond are feasible [20]. Secondly, using narrower WDM spacings and therefore higher channel pair numbers n reduces the number of undesired accidental correlation measurements and therefore enhances the key rate [10]. Deploying WDMs narrower than 100 GHz might require customization, but is possible in principle and also covered by ITU standards [21]. However, going below 6.25 GHz is hardly beneficial anymore. This is because the entangled photons' coherence time is in the order of tens of picoseconds in this case, which deteriorates the timing precision necessary for photon pair correlation. Ultimately, even assuming perfect temporal photon detection, this time-bandwidth product effect represents the physical limit of increasing the rate of polarization and time-bin based QKD protocols [22]. As a side remark, further narrowing the channel width might nevertheless be beneficial in order to address quantum memories for future quantum computing or quantum repeater schemes [23].

In a real-world QKD implementation, where many channels including their respective detection system can terminate at one and the same communication partner, n channel pairs can connect between 2 and $2n$ users individually. However, due to its broad spectrum, our source is also ideally suited for fully connected multi-user quantum network configurations [16]. With the 66 channel pairs available when using 100 GHz spacing, our source could fully connect 12 users in a trusted-node-free network design without any probabilistic multiplexing [24]. Deploying 529 channel pairs of 12.5 GHz width, this number increases to 33 fully connected users.

Although our source is ideally suited for a large variety of applications, its practical deployment is limited by current single-photon detector performance. For calculating the overall key rate, we assume our detector's quantum efficiency, specified to be 80% by the manufacturer, to stay constant for all wavelength channels and count rates. We assume 38 ps jitter of the full detection system including time-tagging electronics, which was the lowest value we observed during our experiment. Most importantly, we have simultaneously assumed maximum detector count rates of 200 MHz. While such count rates can be achieved in state-of-the-art experiments [25], so far there exists no detection system simultaneously exhibiting high detection efficiency and low jitter as well. We note, however, that in (high-loss) long-distant communication scenarios, maximum count-rate limitations do not pose any practical problems for QKD implementations due to the reduced number of registered photons. But also in these cases, low jitter is crucial to avoid accidental two-fold clicks of uncorrelated photons. Thus, it becomes apparent that although recent research shows promising approaches [25–27], detector technology has yet to catch up with high-end entangled-photon-pair sources such as the one presented in this work.

We want to stress that for the claims presented in this

work, no problems or challenges of the source design were shifted to the detection devices. There is no conceivable enhancement to the source that could lead to a QKD performance increase without a significant advance in detector technology first. As of today, detectors are the limiting factor for achieving high key rates: temporal jitter as well as dead time of SNSPDs (and, even more so, of semiconductor-based single-photon detectors) can neither resolve nor register the extraordinarily high pair creation rates of our high-end source.

We have described a source capable of providing more than 1 Gbit/s secure key rate using off-the-shelf components. To the best of our knowledge, this is the brightest source with simultaneously optimized collection efficiency and visibility up to date. Exceptional visibility of the source's polarization-entangled photon pairs enables quantum bit error rates below 0.4 %. Measured collection efficiencies of up to 25.9% provide high photon yield. Damage threshold measurements by the crystal manufacturer [20] suggest that the crystal could be pumped with up to 1 W, which would create more than 10^{11} photon pairs per second over the full spectrum. These exceptional entangled photon pair creation rates cannot be resolved by single-photon detection systems as of today. Thus, we have identified the most pressing problem in current QKD technology as the trade-off between maximum count rate and timing jitter of modern detection systems, which limits the performance of state-of-the-art source technology as presented in this work.

IV. METHODS

A. Source design and working principle

The source is a bulk optics telecom-wavelength source making use of SPDC inside a nonlinear periodically poled 5% magnesium-doped congruent lithium niobate crystal with type-0 phase-matching [28]. The crystal is placed inside a Sagnac loop to enable coherent superposition of orthogonally polarized SPDC modes. The loop was built as small as possible to allow for strong focusing of the pump laser, which has to be carried out by a single lens *outside* the loop in order to be able to separately optimize pump focusing and SPDC collimation. Additionally, using one pump lens benefits indistinguishability of the beam profile in both the loop's propagation direction modes. The focusing parameter ξ was chosen carefully according to efficiency considerations in Ref. [18]. We put emphasis on obtaining a large ratio of crystal length to Rayleigh length of the pump beam in order to obtain high pair creation rates. The comparably strong pump focusing required for this goal can lead to divergence-induced degradation of the PBS extinction ratio, which negatively influences the brightness. We therefore regularly checked the PBS's performance during source construction with lasers at both pump and SPDC wavelength. We selected a nonlinear crystal of 50 mm length

for enabling the SPDC process. In combination with the pump beam's calculated Gaussian profile, this resulted in $\xi = 1.99$. The SPDC beam's focus parameters were matched to the same value as the pump's, which required different collimation and collection parameters due to their different wavelengths. The entangled photons were coupled into an SMF with a 1550 nm anti-reflection coating via an aspheric lens. After passing a longpass filter, all SPDC photons were coupled into one standard SMF-28 single-mode fiber. For a detailed description of the source's working principle, we refer the reader to Fig. 1. Separation of the entangled photon pairs was carried out using standard dense wavelength-division multiplexing (DWDM) modules with a channel spacing of 200 as well as 100 GHz according to the ITU grid. We want to emphasize that we deployed off-the-shelf telecommunication devices for this task. Their spectrum's full width at half maximum (FWHM) amounts to only about 75% of the channel spacing. Deploying custom-made DWDM channels with steeper edges, thus allowing broader FWHM, could therefore increase the usable part of the spectrum by up to 25%. The WDM channels carrying the respective entangled photons of a pair were connected to two channels of a SNSPD system with 80% detection efficiency according to the manufacturer. Detection events were assigned a time stamp with 1 ps bin width by use of a time-tagging module. From two-fold coincident counts between the two detector channels, we calculated a $g^{(2)}$ correlation function for each channel pair. The FWHM of the correlation peak amounted to 38 ps, which is equivalent to the total timing jitter of both detection systems.

B. Benchmarking source performance

To determine the source brightness, i.e. the number of entangled pairs produced via SPDC per second, the WDM channels were connected to the nanowire detectors directly. From their collection efficiencies [17], one can infer the total channel losses and thus the pair production rates (see Fig. 4 and the related discussion). Measurements were carried out for pump powers of 50 μ W to keep the ratio of accidental coincidence counts to pair counts low. Additionally, to check for crystal damages only, we verified source performance for high pump powers of up to 400 mW over high-loss fiber links of 40 dB each. We observed no gray-tracking or other crystal damages up to this power, but chose not to increase it further in order not to risk compromising other experiments the source is needed for.

To determine the source's collection efficiency per nm over its full spectral range, the WDMs were replaced by a 50:50 fiber beam splitter (FBS). One FBS output port was connected to a SNSPD channel directly, while the other one was directed to a free-space rotatable blazed grating reflecting the incoming signal with 1.46 nm/mrad angular dispersion towards an SMF. A 1.25 nm (FWHM) wide portion of the signal was coupled into the SMF,

which effectively acted as a wavelength filter. The SMF was connected to a second SNSPD channel. We determined the ratio between coincident counts of both channels and the single counts of the filter channel for different angle settings of the channel. All measurements were obtained using the same detectors and thus include the SNSPD's wavelength dependency. To account for excess loss due to inefficient coupling and dead-time loss in the first SNSPDs, we normalized for the collection efficiency achieved with the 100 GHz WDMs and thus arrived at Fig. 3.

The entangled photons' state fidelity was measured using two polarization-detection modules with two detector channels each (see Fig. 1). This way, erroneous counts could be quantified directly. The error was determined in two mutually unbiased bases which were set using half-wave plates (HWP). Fidelity measurements were carried out for 7 channel pairs with 200 GHz width and resulted in $> 99.2\%$ visibility, i.e. $< 0.4\%$ QBER for all channel pairs. These values were determined with pump powers low enough to ignore noise-induced coincidence counts, which occurred with probabilities of less than 10^{-4} per registered photon pair. Deploying broader wavelength channels generally leads to lower visibilities, since in-fiber polarization rotations along the WDMs and SMFs leading to the detectors are wavelength-dependent. Thus, compensation using fiber paddles cannot be carried out equally well for the full channel spectrum. Therefore, for the 18.4 nm coarse WDM, the average visibility only reached 90.4%. This problem can easily be mitigated by deploying more WDM channels with denser spacing and individual polarization compensation.

To arrive at the final key rates depicted in Fig. 6, we made use of the model presented in Ref. [8], which was verified with the very same source as the one presented in this work. We used the following input parameters: *Collection efficiencies* were calculated by integrating the function depicted in Fig. 3 over wavelength intervals corresponding to the channel spacings in question. These efficiencies include coupling losses of the source, attenuation in the WDM devices and fibers leading to the SNSPDs, and detection efficiencies of the latter. The *polarization visibility* of at least 99.8% translates to a QBER of 0.4%. For the sake of consistency, we used the *spectral brightness* value $B_{33+35}^{100\text{ GHz}} = 4.10 \times 10^6$ cps/mW/nm of the same 100 GHz channel pair that was used to normalize for the collection efficiency in Fig. 3. The *temporal measurement precision* was assumed to be a convolution of the 38 ps overall detection system jitter with the photons' coherence time, which we approximated from the WDM width in use. Additionally, we assumed a maximum of 2% deadtime-induced loss at 200 MHz *detector count rate*. In our calculation, we ignore post-processing mechanisms such as sifting and finite-key effects and assume perfect error correction and privacy amplification. These are fair assumptions for our high key-rate scenario, since all losses induced by the above effects can be assumed to be negligible for a large

raw key [8].

ACKNOWLEDGMENTS

We acknowledge European Union’s Horizon 2020 programme grant agreement No. 857156 (OpenQKD) and

the Austrian Academy of Sciences in cooperation with the FhG ICON-Programm “Integrated Photonic Solutions for Quantum Technologies (InteQuant)”. We also gratefully acknowledge financial support from the Austrian Research Promotion Agency (FFG) Agentur für Luft- und Raumfahrt (FFG-ALR contract 844360 and 854022).

-
- [1] S. Atzeni, A. S. Rab, G. Corrielli, E. Polino, M. Valeri, P. Mataloni, N. Spagnolo, A. Crespi, F. Sciarrino, and R. Osellame, Integrated sources of entangled photons at the telecom wavelength in femtosecond-laser-written circuits, *Optica* **5**, 311 (2018).
- [2] C.-W. Sun, S.-H. Wu, J.-C. Duan, J.-W. Zhou, J.-L. Xia, P. Xu, Z. Xie, Y.-X. Gong, and S.-N. Zhu, Compact polarization-entangled photon-pair source based on a dual-periodically-poled ti:linbo3 waveguide, *Opt. Lett.* **44**, 5598 (2019).
- [3] W.-Z. Liu, M.-H. Li, S. Ragy, S.-R. Zhao, B. Bai, Y. Liu, P. J. Brown, J. Zhang, R. Colbeck, J. Fan, Q. Zhang, and J.-W. Pan, Device-independent randomness expansion against quantum side information, *Nature Physics* **17**, 448 (2021).
- [4] F. Kaiser, L. Nghah, A. Issautier, T. Delord, D. Aktas, V. D’Auria, M. De Micheli, A. Kastberg, L. Labonte, O. Alibert, A. Martin, and S. Tanzilli, Polarization entangled photon-pair source based on quantum nonlinear photonics and interferometry, *Optics Communications* **327**, 7 (2014), special Issue on Nonlinear Quantum Photonics.
- [5] S. K. Joshi, *Entangled Photon Pairs: Efficient Generation and Detection, and Bit Commitment*, Ph.D. thesis, Phd Thesis at Centre for Quantum Technologies, National University of Singapore (2014).
- [6] Z. Tang, R. Chandrasekara, Y. C. Tan, C. Cheng, K. Durak, and A. Ling, The photon pair source that survived a rocket explosion, *Scientific Reports* **6**, 25603 (2016).
- [7] A. Anwar, C. Perumangatt, F. Steinlechner, T. Jennewein, and A. Ling, Entangled photon-pair sources based on three-wave mixing in bulk crystals, *Review of Scientific Instruments* **92**, 041101 (2021).
- [8] S. P. Neumann, T. Scheidl, M. Selimovic, M. Pivoluska, B. Liu, M. Bohmann, and R. Ursin, Model for optimizing quantum key distribution with continuous-wave pumped entangled-photon sources (2021), in print at *Physical Review A*, arXiv:2103.14639 [quant-ph].
- [9] D. Aktas, B. Fedrici, F. Kaiser, T. Lunghi, L. Labonte, and S. Tanzilli, Entanglement distribution over 150 km in wavelength division multiplexed channels for quantum cryptography, *Laser & Photonics Reviews* **10**, 451 (2016).
- [10] J. Pseiner, L. Achatz, L. Bulla, M. Bohmann, and R. Ursin, *Quantum Science and Technology* **6**, 035013 (2021).
- [11] S. P. Neumann, D. Ribezzo, M. Bohmann, and R. Ursin, Experimentally optimizing QKD rates via nonlocal dispersion compensation, *Quantum Science and Technology* **6**, 025017 (2021).
- [12] K. Heshami, D. G. England, P. C. Humphreys, P. J. Bustard, V. M. Acosta, J. Nunn, and B. J. Sussman, Quantum memories: emerging applications and recent advances, *Journal of Modern Optics* **63**, 2005 (2016), pMID: 27695198.
- [13] Z. Yuan, A. Plews, R. Takahashi, K. Doi, W. Tam, A. W. Sharpe, A. R. Dixon, E. Lavelle, J. F. Dynes, A. Murakami, M. Kujiraoka, M. Lucamarini, Y. Tanizawa, H. Sato, and A. J. Shields, 10-mb/s quantum key distribution, *Journal of Lightwave Technology* **36**, 3427 (2018).
- [14] N. T. Islam, C. C. W. Lim, C. Cahall, J. Kim, and D. J. Gauthier, Provably secure and high-rate quantum key distribution with time-bin qudits, *Science Advances* **3**, 10.1126/sciadv.1701491 (2017).
- [15] T. Zhong, H. Zhou, R. D. Horansky, C. Lee, V. B. Verma, A. E. Lita, A. Restelli, J. C. Bienfang, R. P. Mirin, T. Gerrits, S. W. Nam, F. Marsili, M. D. Shaw, Z. Zhang, L. Wang, D. Englund, G. W. Wornell, J. H. Shapiro, and F. N. C. Wong, Photon-efficient quantum key distribution using time-energy entanglement with high-dimensional encoding, *New Journal of Physics* **17**, 022002 (2015).
- [16] S. Wengerowsky, S. K. Joshi, F. Steinlechner, H. Hübel, and R. Ursin, An entanglement-based wavelength-multiplexed quantum communication network, *Nature* **564**, 225 (2018).
- [17] D. N. Klyshko, Use of two-photon light for absolute calibration of photoelectric detectors, *Soviet Journal of Quantum Electronics* **10**, 1112 (1980).
- [18] R. S. Bennink, Optimal collinear gaussian beams for spontaneous parametric down-conversion, *Physical Review A* **81**, 053805 (2010).
- [19] P. W. Shor and J. Preskill, Simple proof of security of the bb84 quantum key distribution protocol, *Phys. Rev. Lett.* **85**, 441 (2000).
- [20] HC Photonics, “GRIIRA and Laser damage”, <https://drive.google.com/file/d/1qW05mq6-btPuY5uJjaCQ0qEJRAyIHH5P/view>.
- [21] Recommendation ITU-T G.694.1 (2020), “Spectral grids for WDM applications: DWDM frequency grid”.
- [22] Note, however, that deploying high-dimensional degrees of freedom such as orbital angular momentum or path could further increase the bit rate per sent photon.
- [23] Despite efforts to create quantum memories at terahertz bandwidths [29], most current quantum memories exhibit bandwidths of 5 GHz and below [12].
- [24] S. K. Joshi, D. Aktas, S. Wengerowsky, M. Lončarić, S. P. Neumann, B. Liu, T. Scheidl, G. C. Lorenzo, Ž. Samec, L. Kling, A. Qiu, M. Razavi, M. Stipčević, J. G. Rarity, and R. Ursin, A trusted node-free eight-user metropolitan quantum communication network, *Science Advances* **6**, 10.1126/sciadv.aba0959 (2020).
- [25] M. Perrenoud, M. Caloz, E. Amri, C. Autebert, C. Schoenenberger, H. Zbinden, and F. Bussières, Operation of parallel snspds at high detection rate, *Superconductor Science and Technology* (2020).

- [26] T. M. Rambo, A. R. Conover, and A. J. Miller, 16-element superconducting nanowire single-photon detector for gigahertz counting at 1550-nm (2021), arXiv:2103.14086 [quant-ph].
- [27] B. Korzh, Q.-Y. Zhao, J. P. Allmaras, S. Frasca, T. M. Autry, E. A. Bersin, A. D. Beyer, R. M. Briggs, B. Bumble, M. Colangelo, G. M. Crouch, A. E. Dane, T. Gerrits, A. E. Lita, F. Marsili, G. Moody, C. Peña, E. Ramirez, J. D. Rezac, N. Sinclair, M. J. Stevens, A. E. Velasco, V. B. Verma, E. E. Wollman, S. Xie, D. Zhu, P. D. Hale, M. Spiropulu, K. L. Silverman, R. P. Mirin, S. W. Nam, A. G. Kozorezov, M. D. Shaw, and K. K. Berggren, Demonstration of sub-3 ps temporal resolution with a superconducting nanowire single-photon detector, *Nature Photonics* **14**, 250 (2020).
- [28] M. Fejer, G. Magel, D. Jundt, and R. Byer, Quasi-phase-matched second harmonic generation: Tuning and tolerances, *IEEE Journal of Quantum Electronics* **28**, 2631 (1992).
- [29] D. G. England, P. J. Bustard, J. Nunn, R. Lausten, and B. J. Sussman, From photons to phonons and back: A thz optical memory in diamond, *Phys. Rev. Lett.* **111**, 243601 (2013).